A Series Multi-Cells Converter Controlled by Dspace 1103 Using Pid and Fopid Controller Tuning with Gwo and Pso Algorithms: Experimental on Grid-Connected Solar Pv System

Mohamed Redha Skender *[1], Fethia Hamidia [2], Amel Abadi [2], Abdelhalim Tlemcani [2], Faouzi Didi [3] , Moustafa Sahnoune Chaouche [3]

[1]Department of Electrical Engineering/Renewable Energy and Materials Laboratory (REML), Medea University, Algeria.

[2,] Electrical Engineering/Laboratory of Electrical Engineering and Automatics (LREA), Medea University, Aleria.

[3]LERM - Renewable Energy and Materials Laboratory. Department of Common-Core, Faculty of Technology. University of Médéa , 26.000, Algeria

(Corresponding Author): *E-mail: skender.mohamed@univ-medea.dz

Received : 08-01-2023 Accepted: 22-03-2023 Published : 25-04-2023

Abstract

This paper emphasizes the modelling and control of a series multi-cells converter for three phase grid connected PV system. The control strategy applied to the inverter, the fast inner current control loop, which regulates the grid current, and an outer voltage control loop, which controls the dc-link voltage. The control of this inverter for three phase grid connected PV system are designed based on PID and fractional- order PID (FOPID) methods. In this paper the PSO and Grey Wolf Optimizer (GWO) algorithm has been used to tune the parameter of PID and $PI^{\lambda}D^{\mu}$ controller in order to get an optimum time domain specification in which integral of time weighted absolute error (ITAE) has been minimized, where the five parameters (Kp, Ki, Kd, λ and μ) found directly by utilizing (PSO) and GWO algorithm. The design of LCL filter to meet the specified THD requirement for grid is presented and the corresponding harmonic analysis is performed for different methods. The proposed system has been validated using a grid connected three-phase of a series multi-cells inverter. The control algorithm was executed in a dSPACE 1103 real time platform.

Keywords: Nonlinear control, Inverter, Grid-connected solar PV system, Series multi-cells converter, Fractional Order PID-Grey Wolf Optimizer, algorithm, chopper, MPPT-FLC techniques.

Tob Regul Sci. ™ 2023;9(1): 1475-1495
DOI: doi.org/10.18001/TRS.9.1.100

1. INTRODUCTION

Over the last few decades, electronic power converters have undergone significant developments aimed at improving their reliability and efficiency. These advancements are a result of improvements in power electronic components and energy conversion systems. The performance of these converters is directly linked to their topology and power electronic components.

With the growing concerns around global warming and other environmental issues, renewable energy has become a crucial focus of the 21st century. Wind, water, geothermal, and solar energy are increasingly being used for electric power generation. While the use of photovoltaic cells is not new, their effectiveness and convenience have improved significantly and their use has become more widespread.

PV cells operate at maximum power when they are at a specific working point called the maximum power point (MPP). However, this point varies depending on the temperature of the photovoltaic generator and the intensity of insolation. Other factors such as the electrical characteristics of the load, aging of the PV cells, and shading conditions also affect the MPP locus. To ensure that the PV array operates at its MPP regardless of these conditions, a maximum power point tracking network (MPPT) is required. MPPT systems use DC-DC converters with switching modes called choppers and various algorithms such as the Perturb and Observe (P&O) algorithm to control the duty cycle of the converter and maximize power transfer.

Solar energy is used for various applications such as charging batteries and feeding the grid network. Multicell converters are also widely used in electronic devices to convert one form of electrical energy (voltage, current, or frequency) to another. This new topology has the added advantage of modular construction and the use of widely available components.

The model for a multicell converter must strike a balance between simplicity for real-time control and precision for optimal performance. Due to its dependence on both continuous and discrete variables, the model is considered to be delicate [1][2].

Various control methods have been proposed for multicell converters, including nonlinear control based on input-output linearization [3], robust switching control systems with input delay [4], predictive control [5][6], hybrid control [7][8][9], sliding mode control [10][11][12][13], and exponential mapping function [12].

introduced a summarized fractional-order PID (FOPID) controller that includes a λ integral term and a μ derivative term [14]. Compared to the classical PID controller, the FOPID controller provides additional degrees of freedom, making it a popular choice for robust system control. This paper utilizes the Grey Wolf Optimizer (GWO) algorithm [15] to find the optimal

parameters of the FOPID controller, which can minimize the system's performance index. The GWO algorithm is based on the hunting approach of the Canadian grey wolf family [15] and has been developed further in [16]. It adjusts the FOPID controller's parameters to meet time and frequency domain specifications, such as settling time, rise time, maximum overshoot, peak time, gain margin, and phase margin.

Due to the nonlinearity of the PV power systems and their irregular characteristics, the control unit's operating point can shift due to parametric errors and barometric changes. Thus, the primary goal of a grid-connected PV system is to ensure high performance at a low cost by selecting the appropriate control strategy. The control chain consists of two main parts: PVG-side control, which maximizes PVG power using the appropriate MPPT algorithm, and grid-side control, which controls the DC machine voltage and matches the requested power to the grid.

Moreover, FOPID controllers can further enhance the classical PID controller's performance by utilizing the appropriate Fractional-I and Fractional-D actions [17]. To evaluate the feasibility and constraints of the FOPID-GWO techniques, an experimental model is proposed. The model comprises a Dspace1103 card, a three-cell multicellular converter, and an LCL filter, allowing the researchers to define and associate different hardware and software, develop control programs, apply MPPT-FLC techniques for MPPT-PV, and apply FOPID-GWO techniques for controlled multicellular inverter-grid. This paper's main objective is to apply and implement a Fractional Order PID-Grey Wolf Optimizer to the grid-connected multicellular converter connected to the PV system. This control scheme is well-suited for this type of converter and is an effective solution for stabilizing the load against temperature and solar radiation variations. The overall system will be demonstrated through experimentation.

2.MODELLING AND CONTROL STRATEGYOF THE GRID-CONNECTED PHOTOVOLTAIC SYSTEM

The installation's system, as shown in Fig .1, is divided into two stages. The first stage's purpose is to capture solar energy and convert it into direct current using a PV generator connected to a DC-DC boost converter that implements maximum power point tracking (MPPT). The second stage converts the DC into AC using a multicellular series-type three-phase inverter, which sends the alternating current through a low-pass filter to the grid [18].

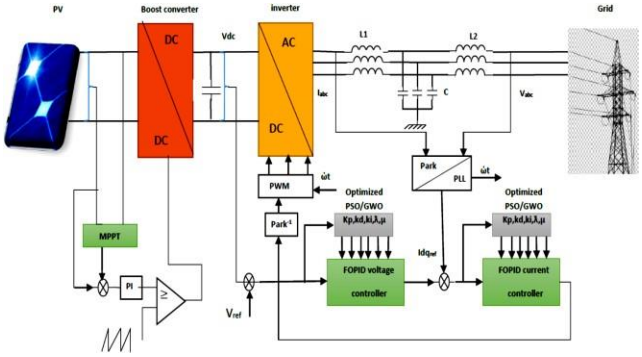

Fig. 1 – Proposed control structure of three phase grid-connected PV system.

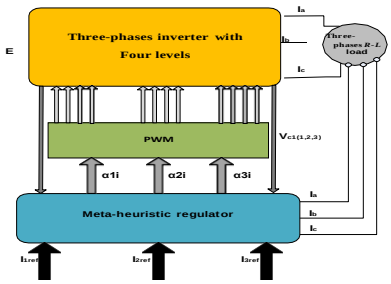

Fig. 2 – Structure PSO control inverter

The inverter is responsible for the following tasks[19].

1. Control of active power supplied to the grid

2. Control of DC link voltage

3. Ensure high quality of injected power

4. Grid synchronization.

The applied control strategy to the inverter, as shown in Fig .2, mainly consists of two cascaded loops, the fast inner current control loop, which regulates the grid current, and an outer voltage control loop, which controls the dc-link voltage.

In this paper, the dq control is chosen.So that the control variables become continuous values. We transform the grid current and voltage waveforms from abc to dq which rotates synchronously with the grid voltage. The parameters of the proposed three phase system are given Table l.

Table 1

Parameters of 3 phase inverter

parameter	value
Grid voltage	230V
Grid frequency	50 Hz
DC link voltage	400V
Switching frequency	1KHz

Output Inverter power	1KVA
Power factor	1
PV output power	100kW

The connected photovoltaic system to the low voltage distribution network supplies only active power, for this the references of the regulators must take the active value (ldre) and the other reactive (lqre), is set to zero whichcorresponds to the output of the inverter.

Hence, the current vector is always in phase with the grid voltage.The phase angle used for the abc to dq transformation module is obtained by the Phase-Locked Loop (PLL).

2.1.PV SYSTEM

PVsystem proposed in this study is mainly equipped with a PVfield of 47 branches linked together in parallel. Each branch consists of 10 PV modules of 100kW. The main parameters characterizing this PVsystem are given in Table 2.

Table 2

Parameters of the PV system

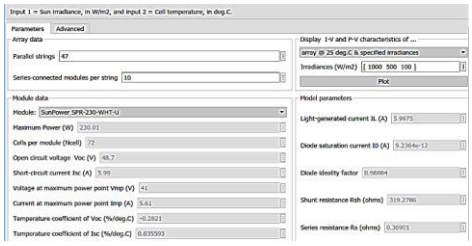

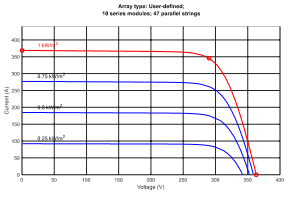

Fig. 3 – Current-voltage characteristics of photovoltaic array at various irradiance levels.

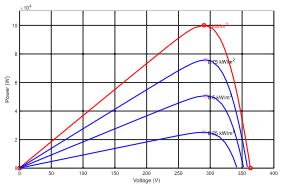

Fig. 4 – power-voltage characteristics of photovoltaic array at various irradiance levels.

2.2. DC / DC CONVERTER

It is ensuredby a booster chopper as shown in Fig .5 whose objective is to design an MPPT control based on artificial intelligence that copes with different atmospheric changes. Considering the impact of insolation and temperature, we propose to analyze the MPPT- Fuzzy logic controller method and evaluate their dynamic behavior in terms of stability, speed and efficiency.

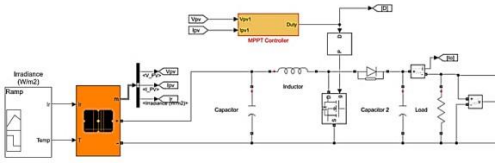

Fig. 5 – booster chopper

MPPT algorithms are fundamental in PV applications on the grounds that the MPP of a solar panel changes with the irradiation and temperature, so the utilization of MPPT algorithms is needed to acquire the maximum power from a solar array.

Over the previous many years' numerous strategies to discover the MPP have been created and distributed. These methods differ in numerous perspectives, for example, the required sensors, intricacy, cost, scope of viability, convergence speed, right following when temperature and/or irradiation change.

For a nonlinear and imprecise mathematical model, the FLC is the best method to control this type as well as it has the advantage of working with imprecise inputs

FLCgenerally consists of three stages:

– Fuzzification: transforms real variables into fuzzy variables.

– Fuzzy Inference System: applies rules to fuzzy inputs (those that were generated by the fuzzification process) to determine fuzzy outputs.

– Defuzzification: it is necessary to transform this fuzzy output information from the Fuzzy Inference System into deterministic information. [20]. The block diagram ofthe FLC is shown in Fig. 6.

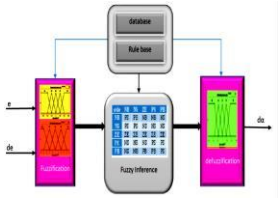

		NS	ZE	PS	PB
NB	PS	PB	NB	NB	NS
NS	PS	PS	NS	NS	NS

ZE	ZE	ZE	ZE	ZE	ZE
PS	NS	NS	NS	PS	PS
PB	NS	NB	PB	PB	PS

Table 3. Rule base.

Fig. 6 – Block diagram of fuzzy logic controller

From the photovoltaic system, the current and the voltage are generated to obtain the error value and the error changes defined in the equation. (1) and eq. (2).

$$E(k) = \frac{P(k) - P(k-1)}{I(k) - I(k-1)} \quad (1)$$

$$\Delta E(k) = E(k) - E(k-1) \quad (2)$$

With E(k) and E(k-1) as the error value at the (k) and (k-1) sampling time respectively, and $\Delta E(k)$ as the changes in error, as well as the value of power (P), and voltage (E) [20]. Fuzzification of error values and changesin error is shown in Fig. 7(a)(b), while duty cycle value is obtained by defuzzification operation is shownin Fig. 7(c). The rule base used are shown in Table 3.

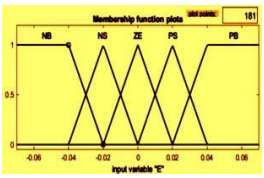

(a) Variable d'entrée E

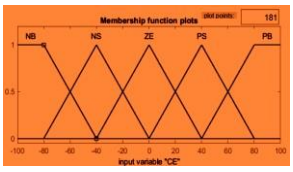

(b) Variable d'entrée Δ_E

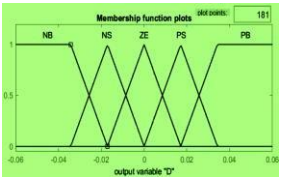

(c) variable de sortie Δ_D

Fig. 7 – Fonctions d'appartenance

2.3. DC / AC CONVERTER

The DC / AC control stage is ensuredby a three-phase multicellular inverter which includes two control loops to improve their efficiency. The inverter regulator includes an internal control loop for DC coupling Voltage (VDC). This voltage control regulates the voltage to its optimum value in order to have the current supplied to the DC link. The second loop is the external control loop for the forward and quadrature currents (Id, Iq) which are supplied by the Phase Locked Loop(PLL). Each of these two loops is controlled by a (FOPID) controller whose gains are modified by applying meta-heuristic techniques (GWO) in order to improve the dynamic performance of the connected PV system to the grid, is to improve the performance of the inverter by modifying the FOPID controllers gains of the current and voltage. For this purpose, there are several meta-heuristic algorithms circulating in the followingsections.

Figure 8 shows the scheme of the proposed system [21]. The control of the converter can be done using a PWM technique. To implement the PWM, two superposed triangular carriers are used. Each carrier is connected to one of the two groups of switches controlled complementarily. The positive part of the carrier fixes the switching state of S1, S2 and S3 whereas the negative part controls S'1,S'2 and S'3. Our objective is to regulate the voltages v_{c1} and v_{c2} of the capacitors to their references $\frac{E}{3}$ and $\frac{2E}{3}$[22].

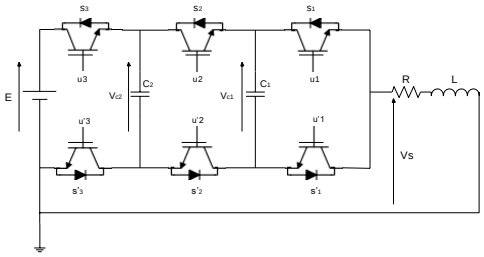

Fig. 8 – Chopper three cells connected to an RL load

The instantaneous state model of a chopper with three cells is expressed as follows:

$$\dot{x}_3 = f_3(x,u) = \begin{matrix} \dot{x}_1 \\ \dot{x}_2 \end{matrix} \quad (3)$$

$(x_1, x_2, x_3)^T = (V_{c1}, V_{c2}, I_{ch})^T$: is the state vector as $x \in \Re^3$

$y = h(x)$: is the measurement vector$y \in \Re$.

(u_1, u_2, u_3) : are controls switches.

$$a_1 = a_2 = \frac{1}{C}, b_0 = \frac{R}{L}, b_1 = \frac{1}{L}, \delta_1 = u_2 - u_1 ,$$

$\delta_2 = u_3 - u_2$: are coefficients.

The control scheme for the three- phase inverter is shown in Figure 9.

Figure 10,11 and Figure 12 present the results of simulation for a series multi cells inverter controlled by the PWM technique, the following command sequence is used[21]:

- The voltage source is 1500V, the reference current is 80A.
- The switching frequency $f_{dec} = 20kHz$
- The capacitance of floating sources$C_1 = C_2 = 50\mu F$
- The frequency of the modulant$f_{mod} = 500Hz$

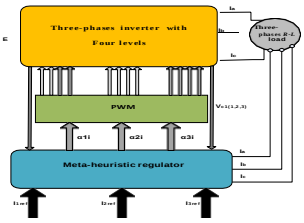

Fig. 9 – Structure PSO control inverter

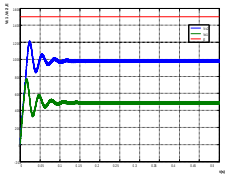

Fig. 10 – Voltage evolutions V_{C1} ,V_{C2} at the capacitors C1 and C2 terminals.

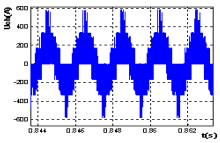

Fig. 11 – the voltage curve U_{ch} at the terminals of the inverter output).

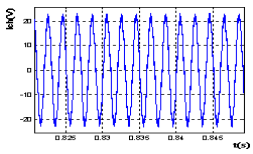

Fig. 12 – the current curve I_{ch} at the terminals of the inverter output).

Our objective is to regulate the voltages v_{c1} and v_{c2} of capacitors to their references $\frac{E}{3} = \frac{1500}{3} = 500V$ and $\frac{2E}{3} = \frac{2\times1500}{3} = 1000V$as shown in Figure 10 and the load current must reach its reference value $I_{ref} = 80A$as shown in Figure 12 .

2.4. GRID-SIDE

For three-phase power systems with sinusoidal voltages and sinusoidal currents, quantities such as

active power, reactive power, active current, and reactive current are conventionally defined on the average concept. But for systems with unbalanced and distorted currents, average concept isnot suitable [23].

In this grid-connected PV system, the effective method is provided to calculate and compensate the reactive power for three-phase systems.

2.4.1.THREE PHASE PLL STRUCTURE

The PLL is used in order to determine the phase angle θ and the frequency of the grid and in this paper, the conventional synchronous reference frame PLL. The block diagram of the used PLL is further shown in Figure.13. A regulator PI is used to control this variable and the output of this regulator is the grid frequency. In this way, the phase angle of grid voltage θ is detected and this is the output of the algorithm.

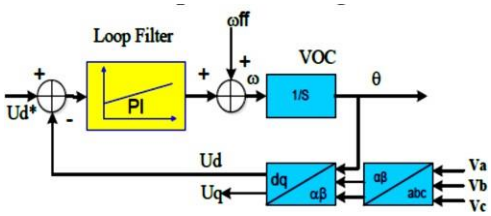

Fig. 13 – Control structure of PLL

2.4.2. FILTER LCL DESIGN

For the L filter, the voltage across the inductor is square. This therefore does not make it possible to have a very sinusoidal voltage at the output. In the LCL case, the input voltage of the inductor is already almost sinusoidal thanks to the LC branch. The LCL filter leads to better attenuation for the same Bandwidth (BP) and better wave quality Figure 14.

A good mention of the LCL filter leads to reduce the high order harmonics on the output side,

However, poor design may cause a distortion increase. Therefore, the filter must be designed correctly and reasonably[24].

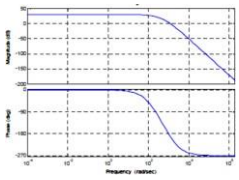

Fig. 14 – Bode diagram of the LCL Filter FT

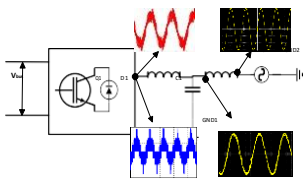

Fig. 15 – Connection through an LCL filter.

Obtained: Li = 4 mH ,Cf = 3 µF, Lg = 2.4 mH ,fres = 2.3 kHz, Rd = 7.5 Ω.

2.4.3. FRACTIONAL-ORDER PID CONTROLLER.

The FOPID

controller control loop feedback mechanism and reduce the error between a measured variable and the desired set point of a process. The generalized transfer function is given by

$$C(s) = \frac{U(s)}{E(s)} = K_P + \frac{K_I}{s^{\lambda}} K_D s^{\mu} \quad (\lambda, \mu \geq 0) \qquad (4)$$

where $C(s)$represents the controller output; $U(s)$ and $E(s)$ are the control signal and the error signal, respectively; The FOPID equation has five unknown parameters, KP, KI, and Kd are the proportional, integral, and derivative constant gains, respectively; λ is the order of integration; and μ is the order of differentiator .If $\lambda = 1$ and $\mu = 1$, a classical PID controller is recovered[25].

The block diagram of control system employing Soft computing FOPID control action is shown in Fig.16.

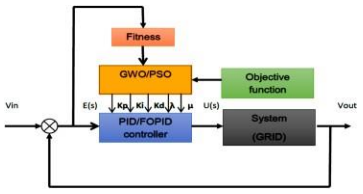

Fig. 16 – A block diagram of Intelligent FOPID controller

where

$V_{in}(s)$: Input Signal

$E(s)$: Error Signal

Vout(s):Output Signal

$U(s)$:Control Signal

– cost function

To evaluate the qualities of the regulator, there are different types of control such as the Integral of Squared Error (ISE), Integral of Absolute Error (IAE), Integral of Time Squared Error (ITSE) , and Integral of Time Absolute Error (ITAE)[26] ..

A drawback of the IAE and ISE categories which influence all errors equally and independent of time) is that they may train in a response with a long settling time and relatively small overshoot [26]. To surmount this disadvantage, an ITAE is used as fitness function.

Therefore, the controller can be evaluated using the following performance index:

$$j(K_p, K_i, K_d, \mu, \lambda) = \int_0^{\infty} t|e(t)|dt \qquad (5)$$

j is called as ITAE. It means that the controlled object is close to the set point model. Where t is the time and $e(t)$ is the error between reference and controlled variable.

2.4.4. Grey Wolf Optimizer algorithm (GWO)

we The FOPID controller is designed and optimized by GWO algorithm. The GWO is a new meta-heuristic algorithm that was invented in 2014 by Seyed Ali Mirjalili[29-31]. GWO is extracted by nature as many other algorithms. To solve the problems of optimization by the GWO, the gray wolves for hunting and their behavior is modeled [29-30].

The GWO algorithm is inspired by the social leadership and hunting behavior of gray wolves in the wild.

To direct the wolves named ω wolves to hopeful areas to find the overall solution. The best solution is to rethink wolves named α, β and δ as leaders

The wolf hunting comprises of three main steps: encircling, hunting, and attacking the prey[29-30].

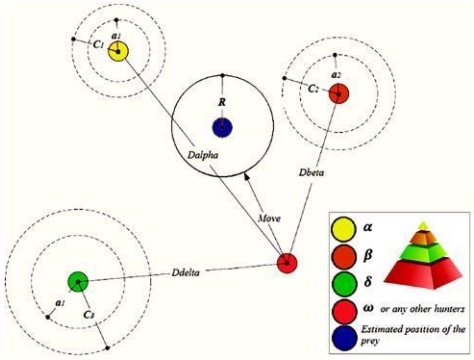

Fig. 17 – The update steps for Grey Wolves Position.

- Encircling: The modeling of The encirclement of the prey by the gray wolves, as shown in Eqs. (6) and (7).

$$D = |C \times X_p(t) - X(t)| \qquad (6)$$

$$X(t+1) = X_p(t) - A \times D \qquad (7)$$

Where X_p is the prey position, X indicates the position vector of a grey wolf, t is the current iteration. C and A are the coefficient vectors calculated by Eqs. (8) and (9).

$$A = 2 \times A \times r_1 - a(t) \qquad (8)$$

$C = 2 \times r_2$	(9)

Where r_1, r_2 are random vectors in [0,1], and the elements of the vector a are linearly decrease from 2 to 0 over the course of iterations by Eq. (10).

$$a(t) = 2 - (2 \times t)/\text{MaxIter} \qquad (10)$$

- Hunting: the modeling of the position of the three best solutions α, β and δ (the other wolves ω are forced to follow them) for the location of the prey. The following Eqs. (11) are described the hunting behavior.

$$\begin{aligned} D_\alpha &= |C_1 \times X_\alpha - X(t)| \\ D_\beta &= |C_2 \times X_\beta - X(t)| \\ D_\delta &= |C_3 \times X_\delta - X(t)| \end{aligned} \qquad (11)$$

Where C1, C2, and C3 are calculated by Eq. (9).

Where $X\alpha$, $X\beta$, and $X\delta$ are the first three best solutions at iteration t, A1, A2, and A3 are calculated

as in Eq. (8), and $D\alpha$, $D\beta$, and $D\delta$ are defined as Eq. (11).

$$X(t+1) = \frac{x_{i1} + x_{i2} + x_{i3}}{3} \qquad (12)$$

- Attacking: the value of a linearly decrease over iterations controls the exploration and exploitation when the wolves launch an attack and the prey stops moving indicating that the hunting process has ended. As shown in Eq. (10), it is updated in each iteration to range from 2 to 0. According to[28] , half of the iterations are dedicated to the exploration, and with a smooth transition, the other half is assigned to exploitation. In this step, wolves change their positions to any random position between the prey position and their current position

Detailed flowchart of the GWO algorithm is shown in Fig. 2.

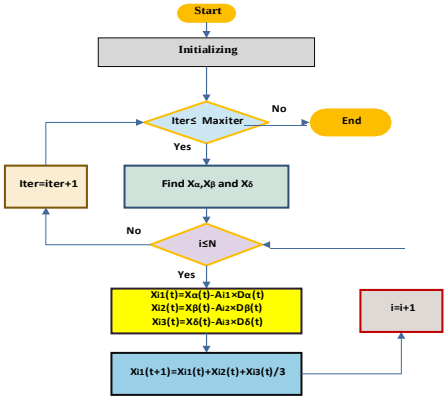

Fig. 18 – The flowchart of the GWO algorithm

Although GWO is simple and applicable for several applications, it suffers from lack of population diversity, the imbalance between the exploitation and exploration, and the premature convergence[27][28][29][30].

2.4.5. PARTICLE SWARM OPTIMIZATION ALGORITHM

Particle swarm optimization (PSO) was proposed by Kennedy and Eberhart in 1995. is believe a school of fish or a flock of birds that moves in a group, it is a simple one to search for an optimal solution in the solution space, it runs until the stop condition is satisfied. The best particle's position gives the optimized parameters for the controller.This is a heuristic solution because we can never prove the real global optimal solution can be found and it is usually not. this optimization algorithm that only the objective function is needed and has very few hyper parameters.

Although GWO is simple and applicable for several applications, it suffers from lack of population diversity, the imbalance between the exploitation and exploration, and the premature convergence[27][28][29][30].

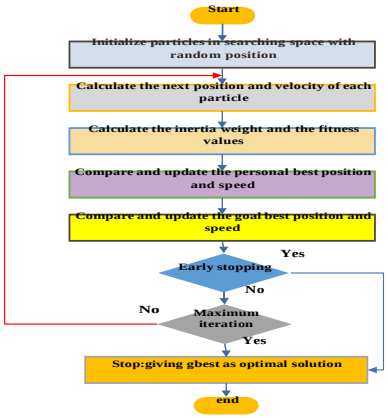

Fig. 19 – Flowchart of PSO algorithm procedure

3. SIMULATION RESULTS AND ANALYSIS

3.1. MPPT methods

in order for the system to have a good characterization of the proposed topology, it was simulated using the Matlab software under different operating conditions, in steady state and in transient state caused by variations in solar radiation[27][31].

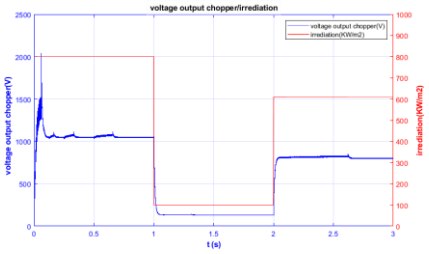

Fig. 20 – DC-link voltage with different irradiations

The simulation is done at the temperature of 250C in three states with three different irradiances. For any T and G as FLC inputs, the output is applied to the chopper control unit, switching pulses are generated so that the PV output voltage is followed by the maximum power point (Vref, mpp). The simulation is shown in Figure 20.

3.2. PID and FOPID controller using PSO and GWO optimizations

From the comparison between (PID-PSO) controller and (PID-GWO) controller in figures21, their performance is almost similar, little difference between them.

for this in the experimental part we choose one of the controllers(PID-GWO) which will be compared with the (FOPID-GWO).

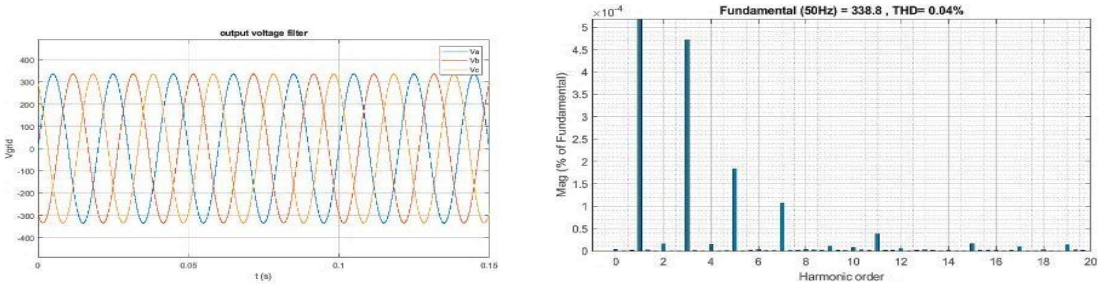

Fig. 21a – Output voltage filter of PID methods .

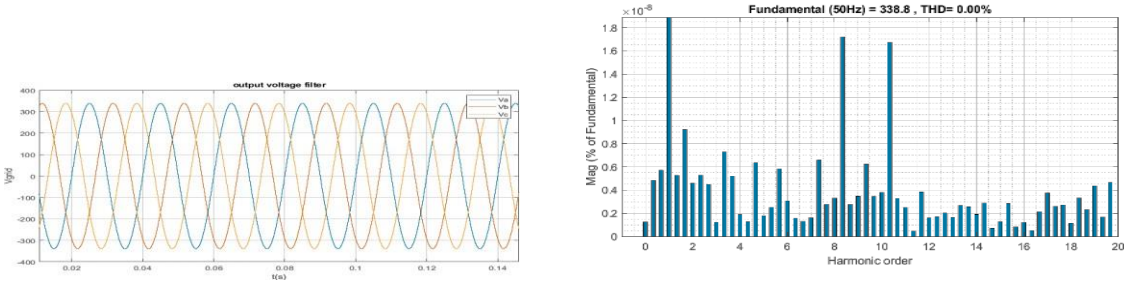

Fig. 21b – Output voltage filter of (FOPID-GOW) methods.

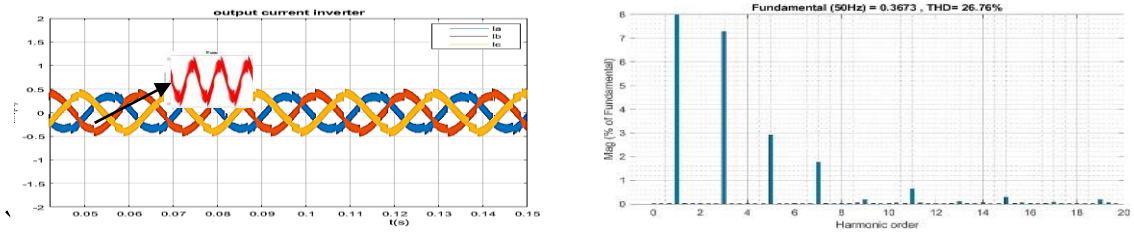

Fig. 21c – Output current filter of PID methods .

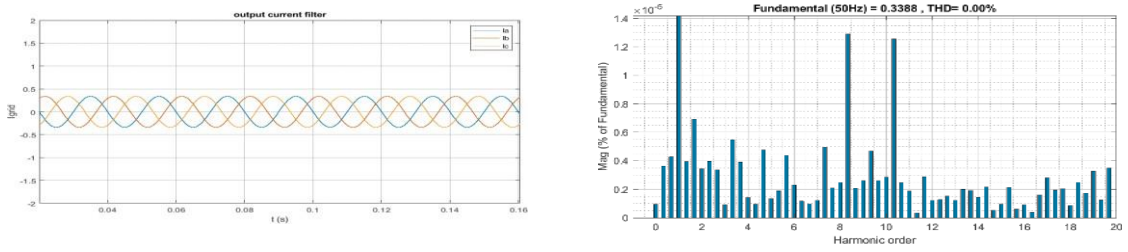

Fig. 21d – Output current filter of (FOPID-GOW) methods.

Fig. 21 – simulation results presents a comparison of PID and (FOPID-GOW) methods

For (PID-GOW) methods the THD is 26,76% as it can be seen on Figure 21c. The load output current from LCL filter is smooth and harmonic analysis show the effectiveness of the designed (FOPID-GWO), the attenuation has been specified for 0% THD on Figure 21.d.

On the other hand, the output voltage shown in Figure 21a, b is very sinusoidal in both cases with better performance in Figure 21.b.

Moreover, the search for the optimal parameters of the FOPID controller here shows that the results are obtained faster and more efficiently by the GWO algorithm than by the PSO algorithm.

The performance characteristics and controller parameters for all controllers are

shown in Tables 4.

Table 4

parameters of controllersalgorithms

algorithms	Kp	Ki	Kd	λ	μ	fitness
FOPID-GWO	400	250	270	0,67	0,63	**0,61**
FOPID-PSO	170,6	592	45,3	0,78	0,10	**1,01**

4.VALIDATION OF ALGORITHM

The experimental results are provided to validate the applicability of the developed techniques and algorithms [32-33].The proposed system has been validated using a grid with LCL filter connected three-phase of a series multi-cells inverter prototype with the ability to operate in a stand-alone mode. The system has been designed and built as shown in Figures 22. The control algorithm was executed in a dSPACE 1103 real time platform.

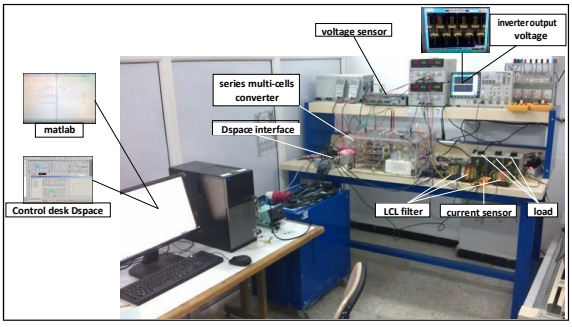

Fig. 22 – **Implementation of the grid with LCL filter connected three-phase of a series multi-cells inverter**

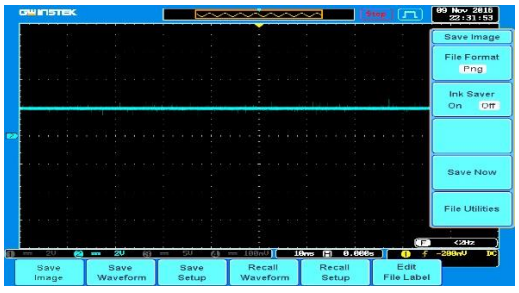

Fig. 23a –V_{c1} Voltage across C_1 capacitor

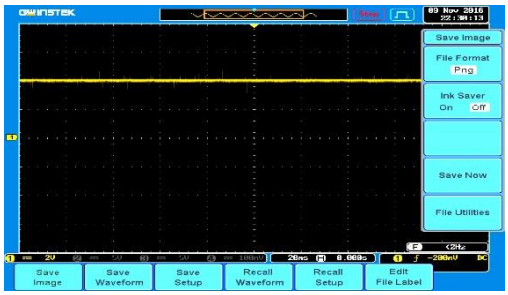

Fig. 23b –V_{c2} Voltage across C_2 capacitor

Fig. 23 – represents the evolution of the floating voltages v_{c1} andv_{c2}

The Figure 23 represents the evolution of the floating voltages v_{c1} andv_{c2} , its voltages quickly evaluate towards the equilibrium state, stabilize at E/3 and 2E/3 respectively. The evolution of the output voltage changes rapidly at the four levels E, 2E/3, E/3 and 0. and for the evolution of

the I_{ch} load current , it is clear that this current is slaved to the reference value.

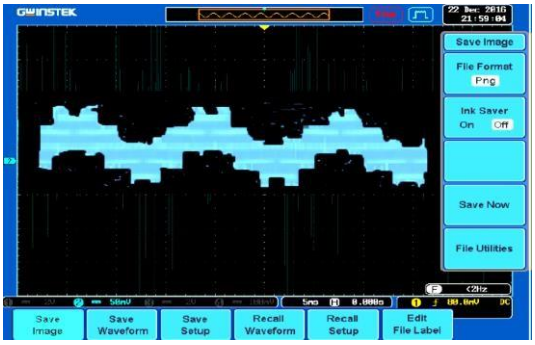

Fig. 24a – Inverter output voltageof PID methods .

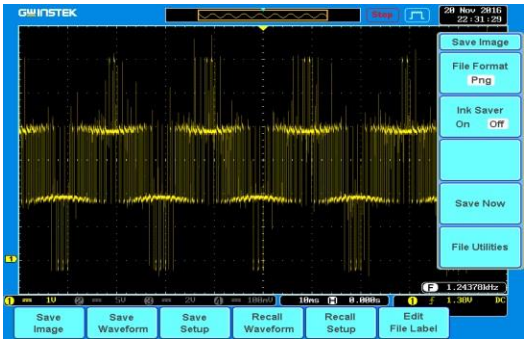

Fig. 24b – Inverter output voltageof (FOPID-GOW) methods..

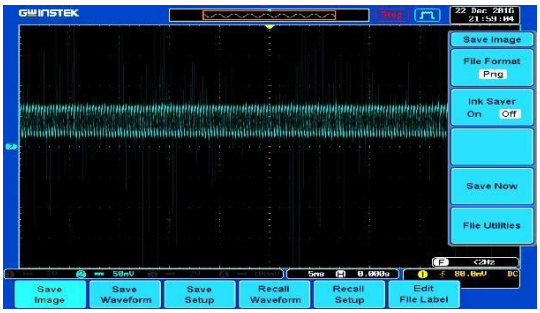

Fig. 24c –load current I_{ch} of PIDmethods

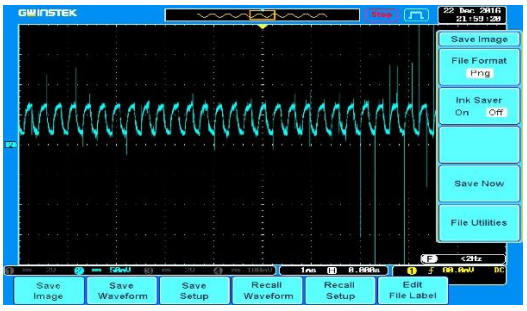

Fig. 24d –load current I_{ch} of (FOPID-GOW) methods.

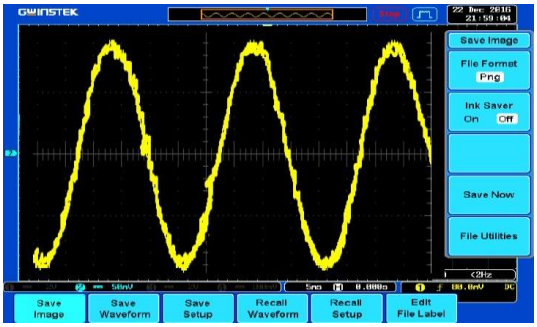

Fig. 24e –Output voltage (after the LCL filter)of PIDmethods .

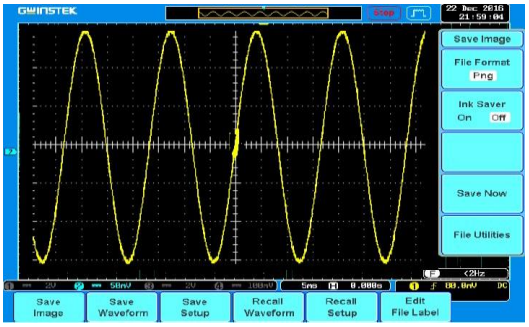

Fig. 24f –Output voltage after the LCL filter of (FOPID-GOW) methods.

Fig. 24 **–experimental results presents a comparison of PID and (FOPID-GOW) methods**

The global system was then verified by experimental results. Fig. 24a through Fig. 24f shows important system variables, captured with an Gwinstek oscilloscope. A SPWM strategy is used in the inverter and the DC link voltage is kept at 400 V. The first set of experimental results obtained output voltage inverter is shown in Fig. 24(a and b), and the second set of experimental

results obtained load current Ich in Fig. 24(c and d), and The output inverter phase-voltage output can be seen in Fig.24(e and f) (after the filter).

For (PID) methods the THD is 26,76% as it can be seen on Fig.24c. The load current output from LCL filter is smooth and harmonic analysis show the effectiveness of the designed (FOPID-GWO), the attenuation has been specified for 0% THD on Fig.24d. In practice the actual value of voltage and current THD is even less than 2%.

5.CONCLUSIONS

This paper presents a detailed study of a three-phase grid-connected solar PV system. The control strategy proposed in this study employs an inner current control loop and an outer DC link voltage control loop. The paper explains the state space modeling of inverter current control and DC link voltage control, and designs the corresponding controllers using PID-PSO/GOW and Fractional Order PID-Grey Wolf Optimizer (FOPID-PSO/GOW) methods. The performance of both methods is evaluated through simulation studies of a grid-connected PV system that uses a three-phase series multi-cells converter (inverter) to connect the PV panel to the grid. The simulation results show that the proposed system is capable of extracting maximum power from the solar PV panels under different irradiation conditions using the proposed MPPT. A 100 kW grid-connected photovoltaic system is used to verify the developed control strategies through simulation studies. The FOPID-GOW control method exhibits a better transient response and settling time, resulting in a stable closed-loop system response. The paper also presents the design of an LCL filter and the calculation of current harmonics using FFT analysis. The simulation results show that the proposed FOPID controller outperforms a conventional PID controller by minimizing trajectory tracking error and reducing control efforts. The effectiveness of the proposed FOPID controllers is verified through different trajectories in MATLAB-Simulink software package and experimental results using Dspace 1103 card. The developed control strategy for the FOPID-GOW control makes the PV system stable under different irradiation conditions.

REFERENCES

1. C. Muro, R. Escobedo, L. Spector, and R. P. Coppinger, Wolf-pack (Canis lupus) hunting strategies emerge from simple rules in computational simulations, Behav. Processes, vol. 88, no. 3, pp. 192–197, Nov. 2011.
2. T. A. Meynard, H. Foch, P. Thomas, J. Courault, R. Jakob, and M. Nahrstaedt, Multicell converters: Basic concepts and industry applications, IEEE Trans. Ind. Electron., vol. 49, no. 5, pp. 955–964, Oct. 2002, doi: 10.1109/TIE.2002.803174.
3. D. Patino, P. Riedinger, and C. Iung, Predictive control approach for multicellular converters, IECON Proc. (Industrial Electron. Conf., vol. 49, no. 5, pp. 3309–3314, 2008.
4. G. Gateau, M. Fadel, P. Maussion, R. Bensaid, and T. A. Meynard, Multicell converters:

Active control and observation of flying-capacitor voltages, IEEE Trans. Ind. Electron., vol. 49, no. 5, pp. 998–1008, Oct. 2002.
5. V. Filipovic, Robust switching control systems with input delay, Stud. Informatics Control, vol. 20, no. 4, pp. 411–420, 2011.
6. F. Defaÿ, A. M. Llor, and M. Fadel, A predictive control with flying capacitor balancing of a multicell active power filter, IEEE Trans. Ind. Electron., vol. 55, no. 9, pp. 3212–3220, 2008.
7. P. Lezana, R. Aguilera, and D. E. Quevedo, Model predictive control of an asymmetric flying capacitor converter, IEEE Trans. Ind. Electron., vol. 56, no. 6, pp. 1839–1846, 2009.
8. M. R. Skender and A. Tlemcani, Application on the series multi-cells converter for implementation and comparison between a higher order sliding mode control and simple order, J. Electr. Electron. Eng., vol. 8, no. 1, pp. 31–36, 2015.
9. M. R. Skender and A. Tlemcani, Sliding mode observer control founded to series multi-cell converter, 2015 4th Int. Conf. Electr. Eng. ICEE 2015, pp. 1–5, Feb. 2015.
10. M. Bâja, D. Patino, H. Cormerais, P. Riedinger, and J. Buisson, Hybrid control of a three-level three-cell dc-dc converter, Proc. Am. Control Conf., pp. 5458–5463, 2007.
11. M. R. Skender and A. Tlemcani, Sliding mode observer control founded to series multi-cell converter | IEEE Conference Publication | IEEE Xplore, IEEE Xplore, Feb. 25, 2016. https://ieeexplore.ieee.org/document/7416842 (accessed Dec. 23, 2021).
12. L. Amet, M. Ghanes, and J. P. Barbot, Direct control based on sliding mode techniques for multicell serial chopper, Proc. Am. Control Conf., pp. 751–756, 2011.
13. M. Djemai, K. Busawon, K. Benmansour, and A. Marouf, High-order sliding mode control of a DC motor drive via a switched controlledmulti-cellular converter, https://doi.org/10.1080/00207721.2010.545492, vol. 42, no. 11, pp. 1869–1882, Nov. 2011.
14. S. Meradi, K. Benmansour, K. Herizi, M. Tadjine, and M. S. Boucherit, Sliding mode and fault tolerant control for multicell converter four quadrants, Electr. Power Syst. Res., vol. 95, pp. 128–139, Feb. 2013.
15. P. I., Fractional-order systems and fractional-order controllers, Slovak Acad. Sci., vol. 12, no. 3, pp. 1–18, 1994.
16. S. D, Empowerment as a New Approach in the Management, Int. J. Account. Bus. Manag., vol. 4, no. 2, pp. 209–221, 2015.
17. A. Badis, M. N. Mansouri, and M. H. Boujmil, Cascade control of grid-connected PV systems using TLBO-based fractional-order PID, Int. J. Photoenergy, vol. 2019, 2019.
18. M. R. Skender, A. Tlemçani, Nouvel Algorithme D'observation A Mode Glissant D'ordre Supérieur Appliqué Au Convertisseur Multicellulaire Série (A New Algorithm Observer Of HigherOrderSliding Mode Applied To SeriesMulticells Converter), Rev. Roum. Des Sci. Tech., vol. 61, no. 2, pp. 126–130, 2016, Accessed:Dec. 19, 2021. [Online]. Available: http://revue.elth.pub.ro/index.php?action=details&id=569.

19. D. Haribabu, A. Vangari, and J. N. Sakamuri, Dynamics of voltage source converter in a grid connected solar photovoltaic system, in 2015 International Conference on Industrial Instrumentation and Control, ICIC 2015, Jul. 2015, pp. 360–365.
20. M. R. Skender,Commandes Non-Lineaires Et Observations D'un Convertisseur Multicellulaire Serie : Theorie Et Experimentation, MEDEA, 2017.
21. M. R. Skender, A. Tlemçani, and H. Nouri, A novel observer algorithm of voltages across capacitors based on the higher sliding mode control: Application to multi-cells converter, Int. J. Model. Identif. Control, vol. 27, no. 2, pp. 136–145, 2017.
22. A. E. W. H. Kahlane, L. Hassaine, and M. Kherchi, LCL filter design for photovoltaic grid connected systems, Third Int. Semin. new Renew. energies, vol. 8, no. 2, pp. 227–232, 2014.
23. J. F. Silva and S. F. Pinto, Linear and Nonlinear Control of Switching Power Converters, Power Electron. Handb., pp. 1141–1220, 2018.
24. A. Idir, Speed Control of DC Motor Using PID and FOPID Controllers Based on Differential Evolution and PSO, Int. J. Intell. Eng. Syst., vol. 11, no. 4, pp. 241–249, 2018.
25. A. Naserbegi, M. Aghaie, and A. Zolfaghari, Implementation of Grey Wolf Optimization (GWO) algorithm to multi-objective loading pattern optimization of a PWR reactor, Ann. Nucl. Energy, vol. 148, p. 107703, 2020.
26. E. Emary, H. M. Zawbaa, and C. Grosan, Experienced Gray Wolf Optimization Through Reinforcement Learning and Neural Networks, IEEE Trans. Neural Networks Learn. Syst., vol. 29, no. 3, pp. 681–694, 2018.
27. A. A. Heidari and P. Pahlavani, An efficient modified grey wolf optimizer with Lévy flight for optimization tasks, Appl. Soft Comput., vol. 60, pp. 115–134, Nov. 2017.
28. W. Long, J. Jiao, X. Liang, and M. Tang, An exploration-enhanced grey wolf optimizer to solve high-dimensional numerical optimization, Eng. Appl. Artif. Intell., vol. 68, pp. 63–80, Feb. 2018.
29. C. Lu, L. Gao, and J. Yi, Grey wolf optimizer with cellular topological structure, Expert Syst. Appl., vol. 107, pp. 89–114, Oct. 2018.
30. Q. Tu, X. Chen, and X. Liu, Hierarchy Strengthened Grey Wolf Optimizer for Numerical Optimization and Feature Selection, IEEE Access, vol. 7, pp. 78012–78028, 2019.
31. M. Hlaili and H. Mechergui, Comparison of Different MPPT Algorithms with a Proposed One Using a Power Estimator for Grid Connected PV Systems, Int. J. Photoenergy, vol. 2016, 2016.
32. M. R. Skender, A. Tlemçan, K. Sebaa, and H. Nouri, Voltages state estimator algorithm of multi-cells converter using sliding mode, 2017 52nd Int. Univ. Power Eng. Conf. UPEC 2017, vol. 2017-Janua, pp. 1–6, 2017.
33. M. R. Skender and A. Tlemcani, Implementation of a new super twisting mode algorithm controlled by dspace: Application to series multicell converter, Stud. Informatics Control,

Mohamed Redha SKENDER et Al
A Series Multi-Cells Converter Controlled by Dspace 1103 Using Pid and Fopid Controller Tuning with Gwo and Pso Algorithms: Experimental on Grid-Connected Solar Pv System
vol. 25, no. 2, pp. 255–264, 2016.